Planta (2004) 218: 501–515
DOI 10.1007/s00425-003-1125-1

ORIGINAL ARTICLE

Marisa S. Otegui · L. Andrew Staehelin

Electron tomographic analysis of post-meiotic cytokinesis during pollen development in *Arabidopsis thaliana*

Received: 13 May 2003 / Accepted: 18 September 2003 / Published online: 11 November 2003

Abstract The mechanism of cell wall formation after male meiosis was studied in microsporocytes of *Arabidopsis thaliana* (L.) Heynh. by means of thin-section and immuno-electron microscopy and dual-axis electron tomography of high-pressure-frozen/freeze-substituted cells. The cellularization of four-nucleate microsporocytes involves a novel type of cell plate, called a post-meiotic-type cell plate. As in the syncytial endosperm, the microsporocyte cell plates assemble in association with mini-phragmoplasts. However, in contrast to the endosperm cell plates, post-meiotic type cell plates arise simultaneously across the entire division plane. Vesicles are transported along mini-phragmoplast microtubules by putative kinesin proteins and, prior to fusion, they become connected together by 24-nm-long linkers that resemble exocyst complexes. These vesicles fuse with each other to form wide tubules and wide tubular networks. In contrast to endosperm cell plates, the wide tubular networks in microsporocytes completely lack callose and do not appear to be constricted by dynamin rings. The most peripheral wide tubular networks begin to fuse with the plasma membrane before the more central cell plate assembly sites become integrated into a coherent cell plate. Fusion with the parental plasma membrane triggers callose synthesis and the wide tubular domains are converted into convoluted sheets. As the peripheral convoluted sheets accumulate callose and arabinogalactan proteins, they are converted into stub-like projections, which grow centripetally, i.e. toward the interior of the syncytium, fusing with the wide tubular networks already assembled in the division plane. We also demonstrate that the ribosome-excluding cell plate assembly matrix is delivered to the mini-phragmoplast with the first vesicles, and encompasses all the linked vesicles and intermediate stages in cell plate formation.

L. A. Staehelin (✉)
Department of Molecular, Cellular, and Developmental Biology,
University of Colorado,
UCB 347, Boulder, CO 80309, USA
E-mail: staeheli@spot.colorado.edu
Fax: +1-303-4927744

M. S. Otegui
Instituto de Fisiología Vegetal,
Universidad Nacional de La Plata,
c.c.327, 1900 La Plata, Argentina

Keywords *Arabidopsis* · Cell plate · Cytokinesis · Electron tomography · Male meiosis · Mini-phragmoplasts

Abbreviations *AGP* Arabinogalactan protein · *MT* Microtubule

Introduction

Higher plants employ several different cytokinetic mechanisms. During "conventional" somatic cytokinesis, cell plates arise right after nuclear division in association with the phragmoplast, a complex array of cytoskeletal elements partially derived from the mitotic spindle (Staehelin and Hepler 1996). Furthermore, the future site of the division plane is defined by the assembly of a preprophase band of microtubules (MTs) before prophase (Mineyuki 1999). In contrast, in some plant cells related to the sexual reproductive phase, new cell walls form by "unconventional" cytokinesis, i.e. cell wall formation is independent of nuclear division (Otegui and Staehelin 2000a). In these systems, multiple cycles of karyokinesis that give rise to multinucleate cells or syncytia precede cytokinesis. Thus, when cytokinesis does take place, multiple cell walls are produced simultaneously between sister and non-sister nuclei. In *Arabidopsis*, unconventional cytokinesis occurs during male and female sporogenesis, and during endosperm and embryo sac cellularizations (Otegui and Staehelin 2000a).

Syncytial cells do not form pre-prophase bands. Instead, new cell walls are positioned at the boundaries of "nuclear cytoplasmic domains", which are defined by arrays of MTs that radiate from the surfaces of the syncytial nuclei (Brown and Lemmon 2001a, 2001b).

The mechanisms postulated to explain how cell walls are formed in syncytial cells have been controversial due to difficulties associated with preserving the cells for ultrastructural analysis and with identifying the structural intermediates. For most syncytial systems at least two different models of cell wall formation have been reported, either by cell plate assembly or by cleavage furrows (reviewed in Otegui and Staehelin 2000a). We have recently solved the controversy surrounding the process of endosperm cellularization in *Arabidopsis* by studying cells preserved by high-pressure freezing/freeze-substitution techniques (Otegui and Staehelin 2000b; Otegui et al. 2001). These studies provided unambiguous proof for the involvement of cell plates in endosperm wall formation. However, there is still no consensus on how cell walls arise after male meiosis during simultaneous cytokinesis.

In different plant species, post-meiotic cytokinesis can occur successively after both telophase I and telophase II, or simultaneously after completion of meiosis. After cell wall formation, the four resulting microspores transiently remain enclosed by a common callose cell wall and upon being released, develop into pollen grains. Based on a large number of studies (Brown and Lemmon 1991b), there seems to be a general agreement that in most dicots undergoing simultaneous cytokinesis, including *Arabidopsis* (Owen and Makaroff 1995), the formation of post-meiotic walls proceeds by cleavage furrows that originate from the parental plasma membrane and grow inward, quadripartitioning the microsporocyte cytoplasm. In some monocots, however, cytokinesis in microsporocytes is reported to involve phragmoplasts and cell plates (some orchids and *Carex*, Brown and Lemmon 1991a, 2000), or cell plates without typical phragmoplasts (in the orchid *Cypripedium*, Brown and Lemmon 1996). If post-meiotic cytokinesis during pollen development in dicots does involve the formation of a cleavage furrow, then this would represent the only known exception to the cell plate-based mechanism of cytokinesis in higher plants.

Genetic and molecular studies in *Arabidopsis* appear to support the hypothesis of a special cytokinetic mechanism operating in microsporocytes. In mutants such as STUD (Hülskamp et al. 1997) and TETRASPORE (Spielman 1997), only cytokinesis after male meiosis is affected, whereas somatic cytokinesis, endosperm cellularization, and female sporogenesis appear to be normal. In addition, KNOLLE, a syntaxin involved in vesicle fusion during assembly of cell plates, both in somatic cells and endosperm, is not detected in microsporocytes (Lauber et al. 1997).

The structural evidence in support of cytokinesis in microsporocytes involving cleavage furrows is based on microscopical observations of chemically fixed samples. Such specimens often exhibit structural distortions that make the interpretation of labile structures difficult. In addition, the limited Z-axis resolution of thin-sectioned specimens makes it nearly impossible to adequately sample variations in cell plate/cleavage furrow architecture throughout a sample. As we have already demonstrated for syncytial-type cell plate formation in *Arabidopsis* (Otegui et al. 2001), all of these problems can be overcome by a combination of cryofixation and dual-axis electron tomography techniques, which provide the means for elucidating the three-dimensional (3-D) architecture of the different types of membrane intermediates, cytoskeletal elements, and the spatial distribution of macromolecular protein complexes such as dynamin rings and kinesin-like proteins in cell plate formation (Otegui et al. 2001).

In this study, we analyze the cytokinetic mechanism that leads to microspore tetrad formation in *Arabidopsis* using high-pressure-frozen/freeze-substituted samples and dual-axis electron tomography at approx. 7 nm resolution. We show that this process is mediated by formation of a unique type of cell plate, which exhibits a *centripetal* pattern of maturation (versus a *centrifugal* pattern of maturation in all other types of cell plate), does not appear to have associated dynamin rings, and has an unusual polysaccharide and glycoprotein composition. In addition, we document the presence of molecules that link vesicles and membranous tubules during cell plate formation and the delivery of the ribosome-excluding cell plate assembly matrix to the division plane together with the vesicles. This report, together with recent studies on high-pressure-frozen/freeze-substituted endosperm samples (Otegui and Staehelin 2000b; Otegui et al. 2001), demonstrates that in different tissues of higher-plant cells cytokinesis can proceed by formation of different types of cell plate but *never* involves cleavage furrows.

Materials and methods

Plant material

Seeds of *Arabidopsis thaliana* (L.) Heynh. (Landsberg *erecta*) were planted in Metro-mix 200 growing medium with *Arabidopsis* controlled-release fertilizer 17-6-12 + minor (Lehle seeds, Texas, USA). Plants were grown in continuous fluorescent lighting, at a temperature of 24 ± 1°C, and a relative humidity of 45%. Developing anthers were excised at various stages before anthesis.

High-pressure freezing and freeze substitution

Whole developing anthers were removed from flower buds and immediately loaded in sample holders filled with 0.1 M sucrose. The samples were frozen in a Baltec HPM 010 high-pressure freezer (Technotrade, Manchester, NH, USA) and then transferred to liquid nitrogen for storage. Substitution was performed in 2% OsO_4 in anhydrous acetone at −80°C for 72 h, and followed by slow warming to room temperature over a period of 2 days. After several acetone rinses, samples were teased from the holders and infiltrated in Epon resin (Ted Pella, Redding, CA, USA) following the schedule: 5% resin in acetone (4 h), 10% resin (12 h), 25% resin (12 h) 50%, 75% and 100% (24 h each concentration). Polymerization was carried out at 60°C. For immunolabeling, some high-pressure-frozen samples were substituted in 0.1% uranyl acetate plus 0.2% glutaraldehyde in acetone at −80°C for 72 h, and warmed to −20°C for 24 h. After several acetone rinses these

samples were infiltrated with London Resin White (Electron Microscopy Sciences, Fort Washington, PA, USA) during 48 h and polymerized at 50°C under vacuum for 24 h.

Immunolabeling of polysaccharides and arabinogalactan proteins (AGPs)

We used a monoclonal antibody to β-1,3-glucan from Biosupplies (Parkville, Victoria, Australia). Xylogucans and methyl-esterified pectins were localized by means of an anti-xyloglucan polyclonal antibody (Moore et al. 1986), and the JIM7 monoclonal antibody (Knox et al. 1990), respectively. Cellulose was identified by means of a probe consisting of cellobiohydrolase I bound to 15-nm gold particles (Krishnamurthy 1999). Cellobiohydrolase was a gift of Dr. Shulein (Novo Nordisk, Danbury, CT, USA). Carbohydrate epitopes of AGPs were identified with the help of three monoclonal antibodies: LM2 (Smallwood et al. 1996), JIM13 (Knox et al. 1991), and MAC207 (Pennel and Roberts 1990).

Sections from samples embedded in Epon (anti-callose, anti-xyloglucans, LM2, JIM13, and MAC207) or in LR White (JIM7) were placed on Formvar-coated nickel grids. The sections were blocked for 20 min with a 5% (w/v) solution of non-fat milk in phosphate-buffered saline (PBS) containing 0.1%Tween-20 (PBST). The primary antibodies, anti-callose (1:50 in PBST), anti-xyloglucans (1:10 in PBST), JIM7 (1:1 in PBST), LM2 (1:20 in PBST), JIM13 (1:20 in PBST), and MAC207 (1:20 in PBST) were applied for 1 h at room temperature. The sections were rinsed in a stream of PBS containing 0.5%Tween-20, and then transferred to the secondary antibody (anti-rabbit IgG 1:50 in PBS containing 0.1%Tween-20) for anti-xyloglucans, anti-mouse IgG for anti-callose, and anti-rat IgG for JIM7, JIM13, LM2, and MAC207) conjugated to 15-nm gold particles for 1 h. Controls were performed by omitting the primary antibody.

At least six sections were incubated with each antibody and cellulose-binding probe, and ten micrographs were taken for immunogold analysis. Gold particles were counted in Golgi stacks, Golgi-derived vesicles, cell plates and cell walls. When the labeling was significantly higher than the background but the average of gold particle density was lower than three per 1 μm^2 of cell wall or lower than two gold particles per organelle, the labeling was considered "very low". Higher gold particle densities were considered as positive labeling.

Sample preparation for electron tomography

250-nm-thick Epon sections were mounted on Formvar-coated copper slot grids and stained with 2% uranyl acetate in 70% methanol and Reynold's lead citrate (2.6% lead nitrate and 3.5% sodium citrate, pH 12). After staining, 15-nm colloidal gold particles were added to both sides of the grid to be used as fiducial markers for aligning the series of tilted images. Finally, the grids were carbon-coated to enhance stability.

High-voltage electron microscopy and acquisition of dual-axis-tilt-series images

The sections were mounted in a tilt-rotate specimen holder and observed in a JEM-1000 HVEM (JEOL) operating at 750 kV. The images were taken at 12,000× from $+60°$ to $-60°$ at 1.5° intervals about two orthogonal axes (Mastronarde 1997) and collected in a Gatan digital camera (Gatan, Pleasanton, CA, USA) that covered an area of 1.4×1.4 μm^2 and had a resolution of 1,024×1,024 pixels, at a pixel size of 1.42 nm. To record larger areas, the digitized images of adjacent squares (4 to 9) were combined into montages, the software controlling the camera and microscope was able to reposition the image and focus the specimen after each tilt, and to collect a montage of overlapping frames at each tilt.

Three-dimensional tomographic reconstruction

The images were aligned using the fiducial markers as previously described (Ladinsky et al. 1999). Tomograms were computed for each set of aligned tilts using the R-weighted back-projection algorithm (Gilbert 1972). Merging of the two single axis tomograms into a dual-axis tomogram involved a warping procedure, rather than a single linear transformation (Mastronarde 1997). This procedure was followed for each of the five analyzed sections. Of the resulting five tomograms, there were two pairs of serial sections. These were aligned with each other and combined as previously described (Ladinsky et al. 1999) in a total reconstructed volume of 2.8×2.8×0.5 μm^3, which consisted of 115 tomographic slices of about 4.3 nm in thickness (compression 1.2×1.2×1.4 in z, pixel size 1.7). The other tomogram corresponded to a reconstructed volume of 4.2×4.2×0.25 μm^3 and yielded 80 tomographic slices of 3 nm. Based on the appearance of the unit membrane bilayer and other ultrastructural features we estimate that the resolution in the x–y plane of our tomographic reconstructions is approx. 7 nm. Due to the limited range of tilt angles, the resolution is 1.3-fold worse in the z-direction, i.e. approx. 8–9 nm (Mastronarde 1997).

Three-dimensional modeling

Tomograms were displayed and analyzed with Imod, the graphical component of the IMOD software package (Kremer et al. 1996) using a Silicon Graphics computer. Membranous structures, MTs, and vesicles were modeled as previously described (Otegui et al. 2001). Since the initial exposure to the electron beam causes some degree of section collapse, we calculated the thinning factor for each tomogram and corrected the tomogram's dimension along the z-axis to obtain accurate proportions for displaying models.

The "image slicer" tool of Imod was used to display and analyze slices extracted from the tomogram in any position or orientation. This tool was particularly useful for studying the morphology of MT ends and the linkers between vesicles and MTs.

Three-dimensional analysis

Using Imodinfo, we calculated the density of ribosomes in 1.25×10^{-4}-μm^3 boxes (relative ribosome density) extracted from the 3-D models between 0–50 nm, 50–100 nm, 100–150 nm, and 150–200 nm from the membrane of different cell plate assembly intermediates. We averaged the relative ribosome density of 15 boxes for every cell plate stage and distance from the plasma membrane.

Results

This study, which reports on how cell walls are formed after male meiosis in *Arabidopsis*, is based on results obtained by conventional and immuno-electron microscopy, and by dual-axis high-voltage electron tomography of high-pressure-frozen/freeze-substituted samples containing cellularizing microspore tetrads.

A four-nucleate syncytium forms after male meiosis

In *Arabidopsis*, the microsporogenous tissue inside the anther consists of two to three layers of cells surrounded by the tapetum. Prior to meiosis, microsporocytes are connected to each other and to the tapetal cells through plasmodesmata. When microsporocytes enter into mei-

osis, they deposit a layer of callose between the plasma membrane and the primary cell wall, which causes the plasmodesmatal connections between microsporocytes and tapetal cells to rupture. After this cytoplasmic uncoupling of tapetal and microsporocytes is completed, the plasmodesmatal connections between the microsporocytes enlarge during meiosis and allow the trafficking of cytoplasm and organelles between contiguous microsporocytes (data not shown).

After the first meiotic division, no cell wall is formed between the resulting nuclei. However, the two cytoplasmic domains become clearly separated by the accumulation of mitochondria and plastids at the equatorial plane in an arrangement called the ''organelle band'' (Brown and Lemon 1996; Fig. 1a). The second-division spindles then form at both sides of the organelle band (Fig. 1b). At the end of meiosis, a four-nucleate syncytium is formed (Fig. 1c) and the organelles re-distribute uniformly across the cytoplasm (Fig. 1c).

Cytokinesis involves the simultaneous formation of multiple cell plate assembly sites across the entire division plane

The four haploid nuclei resulting from meiosis re-locate in a tetrahedral arrangement inside the microsporocyte (Fig. 1c,d). Cellularization begins with the simultaneous assembly of six cell plates between the four nuclei at the boundaries of adjacent nuclear cytoplasmic domains (Fig. 1d). Our 3-D tomographic reconstructions show that between a given pair of nuclei, clusters of MTs give rise to individual cell plate initials (Figs. 2, 3). Because these MT clusters resemble those involved in syncytial-type cell plate assembly in the endosperm (Otegui and Staehelin 2000b), we have also named them mini-phragmoplasts. However, unlike those of the endosperm cells, the mini-phragmoplasts in microsporocytes form simultaneously across the entire division plane, and not only in the central region (Figs. 1d, 2). This means that some mini-phragmoplasts give rise to cell plates in close proximity to the parental plasma membrane (Fig. 2). This feature has important implications for the subsequent progress of the cytokinetic process as will be discussed below.

Every mini-phragmoplast consists of 2–12 MTs (Figs. 2, 3), and the mini-phragmoplasts across a given division plane are spaced on average 0.6 μm apart from each other. Vesicles of approx. 48 nm in diameter are seen in close association with mini-phragmoplast MTs (Fig. 3). We have also observed actin filaments interspersed between mini-phragmoplast MTs (Fig. 3c), although in very low quantities due to the fact that the substitution and staining protocols used in this study were optimized for membrane staining and not for actin cytoskeleton visualization.

To analyze the connection between vesicles and MTs we used the ''slicer'', a tool from the Imod program that allows the observation of tomographic slices parallel to the MT main axis. In the reconstructed models we observed that vesicles are connected to MTs by one or two (rarely three) 30-nm bridging structures (Fig. 3a). We have detected similar structures during the assembly of syncytial-type cell plates (Otegui et al. 2001) and, based on their size, their general morphology (Hirokawa et al. 1989), and the fact that the vesicles are being transported towards the plus end of the MTs, concluded they are kinesin-like molecules involved in vesicle transport along MTs.

The density of vesicles in the equatorial plane of the mini-phragmoplast sites varies greatly. Whereas some mini-phragmoplasts contain very few or no vesicles, others show very high densities of vesicles (see Fig. 2). In these later mini-phragmoplasts, up to 14 cell plate-forming vesicles were observed in close proximity (e.g. within 10–30 nm) to a 0.25-μm-long segment of MTs.

Filamentous structures link vesicles and membranous tubules prior to fusion

By using the 'slicer' tool from the Imod program we have been able to identify characteristic filamentous structures

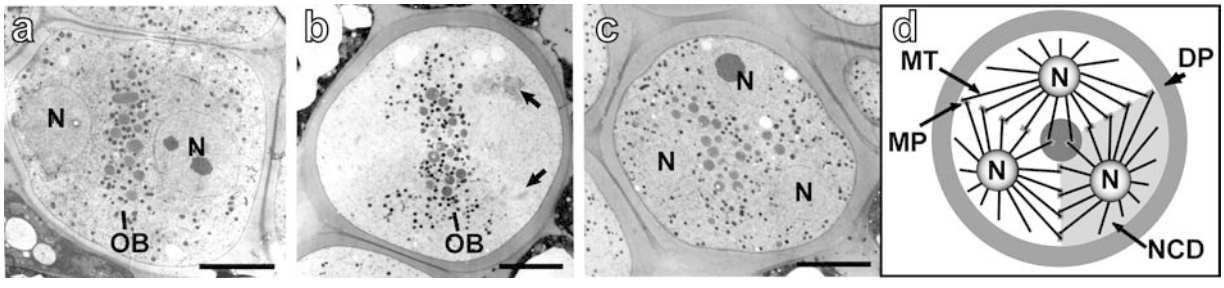

Fig. 1a–d Meiosis and nuclear cytoplasmic domain organization in microsporocytes of *Arabidopsis thaliana*. **a–c** Thin-section electron micrographs of microsporocytes undergoing meiosis. **a** After Telophase I, plastids and mitochondria accumulate between the two resulting nuclei (*N*), in an arrangement called the ''organelle band'' (*OB*). **b** Anaphase II–Telophase II. Meiotic spindles are seen at both sides of the OB. *Arrows* indicate the condensing chromatin. **c** After Telophase II, a four-nucleate syncytium is formed. Only three of the four nuclei (*N*) can bee seen in this micrograph. **d** Diagram showing the organization of the syncytial microsporocyte into nuclear cytoplasmic domains (*NCD*) defined by radial systems of MTs at the onset of the post-meiotic-type cell plate assembly. Note that the mini-phragmoplasts (*MP*) are formed simultaneously across the entire division plane (*DP*). In total, six cell plates assemble in the four-nucleate microsporocyte. Bars = 1 μm (**a–c**)

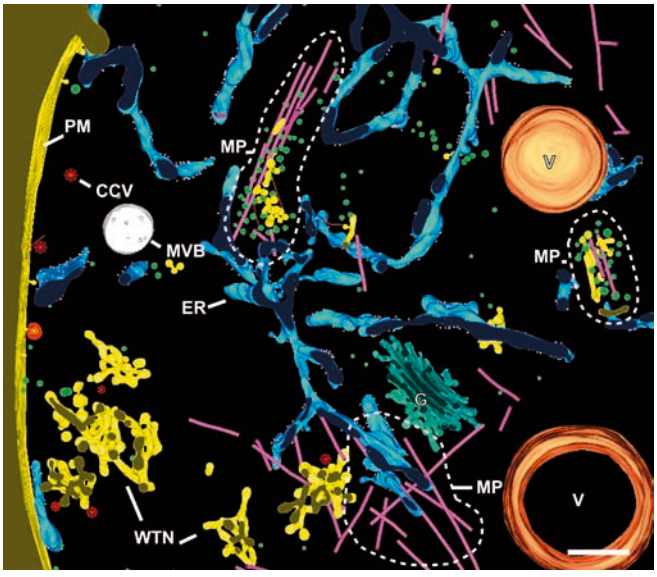

Fig. 2 Three-dimensional tomographic modeled reconstruction of an early post-meiotic cell plate in an *Arabidopsis* microsporocyte. This 4.2×4.2×0.25 μm^3 volume includes a tangential section of the division plane where a post-meiotic cell plate is assembling. Multiple mini-phragmoplasts (*MP*) are distributed across the division plane. Some wide tubular networks (*WTN*) have consolidated in close proximity to the parental plasma membrane (*PM*). Note that the mini-phragmoplast in the bottom of the figure has no associated vesicles. Endoplasmic reticulum cisternae (*ER*), multivesicular bodies (*MVB*), vacuoles (*V*), and a Golgi stack (*G*) are interspersed between mini-phragmoplasts. In addition, a total of 21 mitochondria were found in this tomographic volume but not included in the figure to facilitate the visualization of cell plate assembly sites. *CCV* Clathrin coated vesicles. Bar = 500 nm

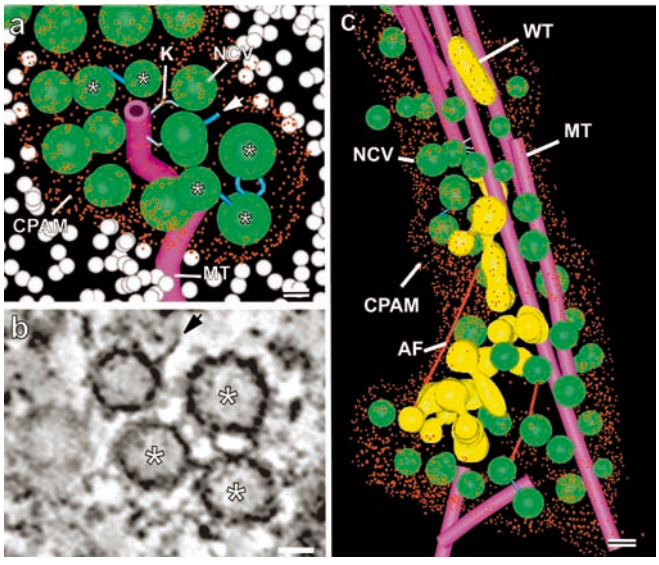

Fig. 3a–c Tomographic analysis of mini-phragmoplasts and associated structures in an *Arabidopsis* microsporocyte. **a** Tomographic model of mini-phragmoplast MTs and associated non-coated vesicles (*NCV*) surrounded by the cell plate-assembly matrix (*CPAM*). The limit of the matrix is indicated by *red stippling*. Two vesicles are connected to the MTs by 30-nm-long, kinked linkers (*K*), likely kinesin molecules (see Otegui et al. 2001). In addition, some vesicles (indicated by *asterisks*) are connected to each other by 24-nm-long linkers (*blue*). The *arrow* indicates one of these linkers with one end free, not attached to a vesicle. A cell CPAM encompasses free vesicles, kinesin-like molecules, and membrane-linkers. **b** A 17.2-nm-thick tomographic slice (slicer views of four integrated 4.3-nm slices) corresponding to a portion of the model showed in **a**. Note the filamentous structures that connect the three vesicles (*asterisks*) as well as a potential linker with an unattached end (*arrow*). **c** Tomographic model of a mini-phragmoplast consisting of MTs, actin filaments (*AF*), and associated non-coated vesicles (*NCV*) and wide tubules (*WT*). Note that most vesicles and tubules are located inside the cell plate-assembly matrix (*CPAM*). Bars = 25 nm (**a**,**b**) 50 nm (**c**)

that connect the cell plate-forming vesicles to each other and to tubular cell plate intermediates (Fig. 4a–f). Approximately 20 of these structures with a bridging length of 24 ± 1 nm have been unambiguously identified in our tomographic reconstructions. Of the vesicles displaying linkers, most appear to posses one bridging structure, while some display two (Figs. 3a,b, 4a–f). In rare cases, structures similar in size and morphology are seen with one end attached to the surface of a vesicle and the other end, free (Fig. 3a,b, arrows). Groups of up to three vesicles are seen interconnected by linkers (Fig. 4-a,b,d,e). These molecules also link vesicles to tubule ends (Fig. 4c,f). Since linked vesicles are seen in the equatorial plane of the cell plate-forming region prior to vesicle fusion, the bridging structures appear to be involved in bringing vesicles and tubules together prior to fusion.

When the accumulated vesicles in the division plane begin to fuse with each other they give rise to different types of vesicle fusion intermediates depending on the number of vesicles coalescing at a given time. Thus, when two vesicles fuse together, hourglass-shaped intermediates are formed (Fig. 4g). An example of three coalesced vesicles is illustrated in Fig. 4h, and a vesicle fused to a tubule is depicted in Fig. 4i. The similarity in architecture of groups of linked vesicles and coalesced vesicles and tubules (compare Fig. 4d–f and Fig. 4g–i) lends further support to the idea that the tethering of vesicles precedes their fusion. The 40- to 50-nm-wide tubules formed by the fusion of vesicles appear to give rise to the typical wide tubular networks illustrated in Figs. 2 and 5.

A cell plate assembly matrix that excludes ribosomes is delivered to the division plane together with the first vesicles

Previously, we have shown that a dense, ribosome-excluding matrix surrounds the early membrane intermediates of developing syncytial-type cell plates (Otegui and Staehelin 2000b; Otegui et al. 2001). We have also detected a similar matrix encompassing all the assembly intermediates during post-meiotic cell plates (Figs. 3, 5). By quantifying in our tomographic reconstructions the density of ribosomes at different distances from the cell plate surface during different stages of cell plate assembly, we have been able to determine when the matrix

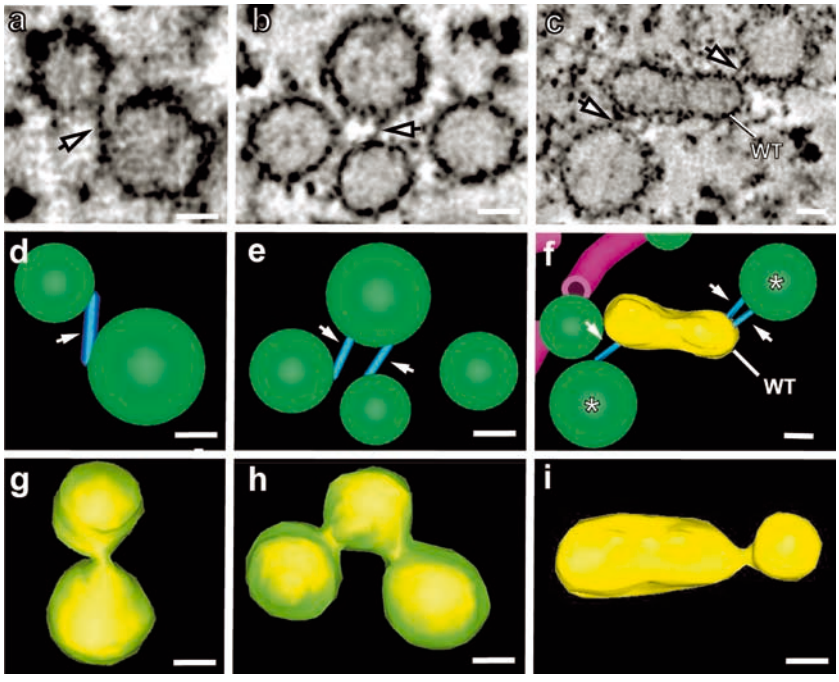

Fig. 4a–i Vesicle-linkers and vesicle fusion intermediates in an *Arabidopsis* microsporocyte. **a–c** Views of 12.9-nm-thick tomographic slices (slicer views of three integrated 4.3-nm slices) through mini-phragmoplast-associated vesicles connected to each other and to wide tubules (*WT*) by bridging structures (*arrows*). **d–f** Three-dimensional tomographic models of the same structures depicted from **a** to **c**. Note that in **c** and **f** a WT is connected to two vesicles (*asterisks*) by bridging structures. **g–i** Three-dimensional tomographic models of vesicle fusion intermediates. Note that the structure depicted in **g** appears to derive from the fusion of two vesicles, the structure in **h**, from the fusion of three vesicles, and the one in **i** from the fusion of a WT with a vesicle. Bars = 25 nm

forms and when it disappears (Fig. 6). Our data indicate that assembly of the matrix starts with the arrival of the first cell plate-forming vesicles at the division plane (Fig. 3a,c), but not before, since no matrix could be detected in mini-phragmoplasts devoid of vesicles. Interestingly, the filamentous structures that link vesicles and membranous tubules are only found inside the limits of the matrix (Fig. 3a).

The matrix persists around the forming cell plate until it reaches the late convoluted sheet stage of development (Figs. 5, 6). In Fig. 6 the density of ribosomes contained in 1.25×10^{-4} μm^3 volumes is plotted against their distances from the surface of different cell plate intermediates (free vesicles, wide tubular networks and convoluted sheets) and from the completed cell wall. The density of ribosomes within a 50-nm distance from the surface of free vesicles, wide tubular networks, and early convoluted sheets is lower than for a completed cell wall. Beyond 50 nm from the cell plate membrane, the ribosome density is the same as in the cytoplasm areas not associated to cell plate assembly (Fig. 6).

Fusion of wide tubular networks to the parental plasma membrane triggers their conversion into convoluted sheets and activates callose synthesis

Wide tubules result from the fusion of cell plate-forming vesicles with each other and grow by the fusion of additional vesicles with the tubules and the fusion of wide tubules with each other. Together, all of these fusion events generate the characteristic wide tubular networks illustrated in Figs. 2, 5, and 7. In contrast to endosperm syncytial-type cell plates (Otegui et al. 2001), no dynamin rings were seen pinching the wide tubular networks of the post-meiotic microsporocytes. These wide tubular networks also do not contain any callose (see below).

As mentioned above, mini-phragmoplasts form simultaneously across the entire division plane and some wide tubular networks develop very close to the microsporocyte parental plasma membrane (Figs. 2, 7). As these tubular domains expand, they reach the plasma membrane and fuse with it before they link up with the tubular networks near the center of the cell (Fig. 8a). It is important to note that this fusion event connects the parental plasma membrane, which is actively synthesizing callose, to the cell plate membrane, which is not. However, once the two membrane systems have fused, callose also begins to accumulate in the wide tubular network and to induce its transformation into a convoluted sheet. Accompanying these events is the appearance of numerous clathrin-coated buds on the transforming membranes (Fig. 8a). The final result of these activities is the presence of more-mature cell plate domains (convoluted sheets) at the cell periphery, and of less-mature domains (wide tubular networks and vesicle

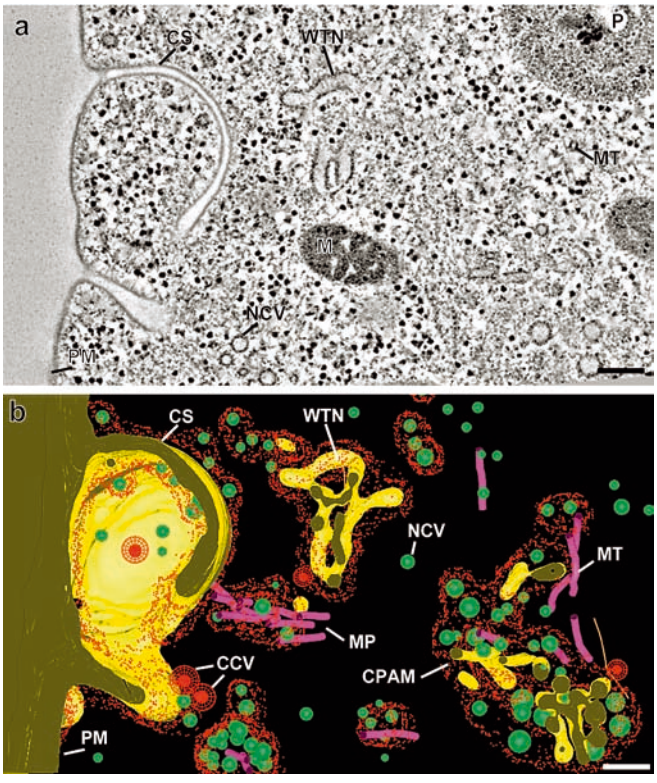

Fig. 5a, b Tomographic analysis of membrane intermediates during cell plate formation and their cell plate-assembly matrixes. **a** A 4.3-nm-thick tomographic slice through a forming cell plate. **b** Tomographic model derived from the tomogram depicted in **a**. The main structures seen in this reconstructed tomographic model include a convoluted sheet domain (*CS*) that is continuous with the parental plasma membrane (*PM*), mini-phragmoplasts (*MP*), non-coated vesicles (*NCV*) and wide tubular networks (*WTN*) encompassed by distinct cell plate-assembly matrixes (*CPAM*) that exclude ribosomes. The mitochondrion (*M*) and plastid (*P*) shown in **a** have not been included in the model to facilitate the visualization of cell plate assembly sites. *CCV* Clathrin-coated vesicles. Bars = 100 nm

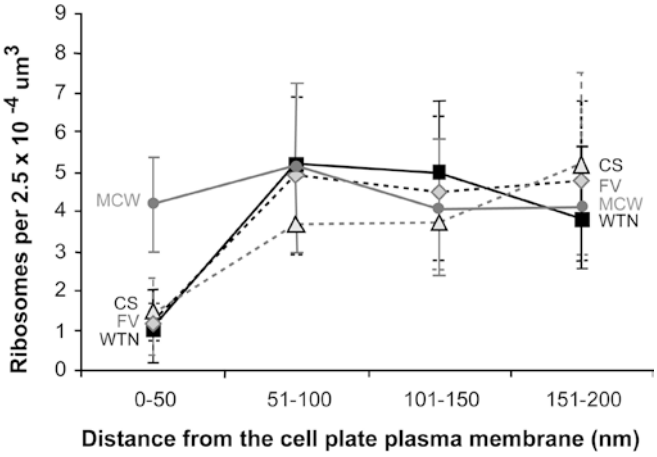

Fig. 6 Changes in ribosome density as a function of distance from the cell plate surface during microsporogenesis in *Arabidopsis*. The densities of ribosomes in the reconstructed volumes are plotted against their distance from the surface of the different cell plate intermediates. *FV* Free vesicles, *CS* convoluted sheet, *MCW* mature cell wall, *WTN* wide tubular network. Errors bars indicate the standard deviation

clusters) towards the center of the microsporocyte (Figs. 5, 8b,c).

Both conventional microscopy and electron tomography were required to analyze the complex architecture of convoluted sheets. The 3-D tomographic reconstructions have demonstrated that convoluted sheets show few openings or fenestrae (Figs. 5b, 9b). Often, those convoluted sheet domains located in the vicinity of cytoplasmic channels have a much more intricate and often layered conformation, and stub-like projections of the plasma membrane are frequently seen to form in their vicinity (Figs. 8c, 9).

The cytoplasmic channels, which connect adjacent microsporocytes, become smaller during cytokinesis, from 0.5 μm in diameter at the beginning of meiosis I (data not shown) to approximately 0.2 μm at the time that convoluted sheets develop (Fig. 8c), and they close completely when cytokinesis is completed.

Cell plate growth occurs by fusion of wide tubular networks in the division plane with the callose-containing cell wall projections

Eventually, all of the convoluted sheet domains fused to the plasma membrane become converted into stub like projections, which expand towards the interior of the syncytium by fusion with the remaining wide tubular networks in the interior of the cell (Fig. 10). Since most of the membrane needed to build a cell plate is already in the division plane, the next steps in cell wall formation appear to occur very quickly as evidenced by the fact that it has been very difficult to find these intermediates in our samples (approx. 200 cells). As the wide tubular networks become incorporated into the thick stub-like projection growing from the plasma membrane, they are transiently converted into convoluted sheets and then into a more planar sheet that matures into the cell wall. During these processes, callose and AGPs are deposited in the cell plate, and excess membrane appears to be removed by clathrin-coated vesicles.

Finally, the sheet-like projections of the six cell plates developing in each microsporocyte merge and fuse together in the central region of the syncytium giving rise to a tetrad of microspores (Fig. 10b). The new cell walls formed between adjacent microspores are approx. 0.5 μm thick, exhibit a homogenous appearance, and completely lack plasmodesmata (Fig. 10b). No middle lamella is observed between microspores in the same tetrad (Fig. 10b).

Post-meiotic cell plates and microsporocyte cell walls have an unusual composition

We have used EM immunolabeling techniques to test for the presence of different polysaccharides and AGPs in

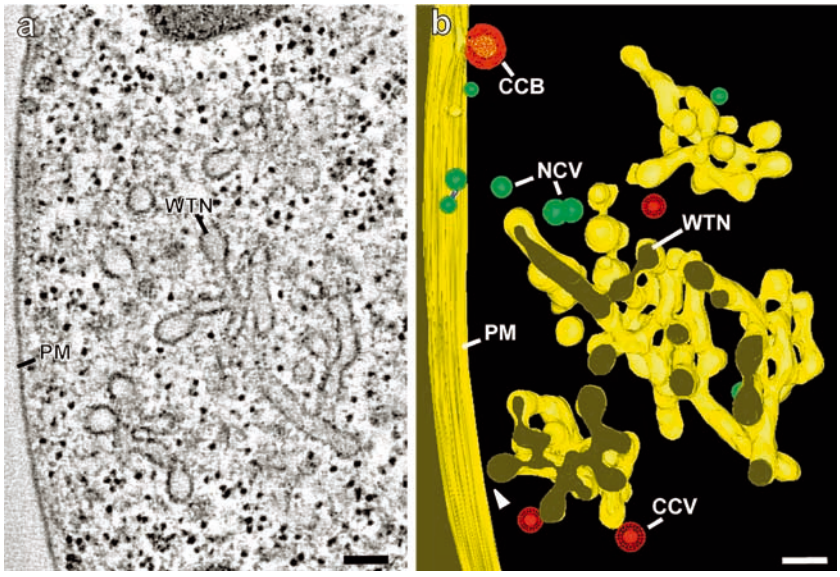

Fig. 7a, b Tomographic analysis of a wide tubular network in an *Arabidopsis* microsporocyte. **a** A 6-nm-thick tomographic slice (slicer views of two integrated 3-nm slices) through wide tubular networks (*WTN*) forming close to the plasma membrane (*PM*). **b** Tomographic model derived from the tomogram depicted in **a**. Note the absence of constricting dynamin-like rings in the WTN membranes. Both non-coated vesicles (*NCV*) and clathrin-coated vesicles (*CCV*) are abundant in this area. *CCB* Clathrin-coated bud. Bars = 100 nm

Golgi stacks, cell plate-forming vesicles, and post-meiotic cell plates of cellularizing microsporocytes, as well as in recently formed cell walls of young microspore tetrads. In addition, we have analyzed the composition of both microsporocyte primary cell wall/middle lamellae and the callosic cell walls, which are deposited when microsporocytes enter into meiosis (Table 1). In our thin sections, the primary cell wall/middle lamella region of the microsporocyte walls can be clearly seen in anthers undergoing meiosis as a darker zone located between the adjacent callosic microsporocyte cell walls (Fig. 8c).

Labeling with an anti-xyloglucan (XG) antibody produced extremely low levels of gold labeling over Golgi-derived vesicles, cell plates, callosic cell walls and microsporocyte primary cell walls (data not shown). To determine if this low anti-XG labeling in the microsporocyte was due to the inability of the antibody to bind to the epitopes in the plastic sections, we used as positive control the cell walls of the surrounding anther tissues (tapetal and anther walls). In those cell walls, a typical heavy anti-XG labeling was observed (data not shown). Thus, both the primary and the callosic cell walls of microsporocytes appear to be essentially devoid of XG.

Callose was detected by means of a monoclonal anti-callose antibody. Microspore callosic cell walls gave a very heavy labeling as expected (Fig. 11a,b). In post-meiotic cell plates, callose was not detected in wide tubular network domains (Fig. 11a), but was pronounced in the convoluted sheets and the stub-like projections, i.e., in the structures formed after fusion of the most peripheral cell plate domains to the parental plasma membrane (Fig. 11b). Callose labeling was also abundant in the recently deposited cell walls of young tetrads. The microsporocyte primary cell wall/middle lamella does not contain callose (Fig. 11b).

The presence of cellulose was assessed by means of the cellulose-binding probe cellobiohydrolase I–gold (CBHI–gold). No cellulose was detected in cell plates or microsporocyte cell walls (data not shown). Once again, the positive labeling of cell walls in tapetal cells was taken as a positive control to assure the probe was effectively binding cellulose in our plastic sections (data not shown).

To assess the content of methyl-esterified pectins we used the JIM7 monoclonal antibody. We obtained very scarce labeling on cell plates, newly formed cell walls, and microsporocyte callosic cell walls. However, microsporocyte primary cell wall/middle lamellae gave a strong labeling pattern (Fig. 11c).

Due to the virtual absence of cellulose, xyloglucans and methyl-esterified pectic polysaccharides in the post-meiotic cell plates and newly formed microspore cell walls, we also tested for the presence of AGPs using antibodies that recognize different epitopes of their glycosidic domains. The LM2 monoclonal antibody, which recognizes a carbohydrate epitope containing glucuronic acid residues (Smallwood et al. 1996), showed the same labeling pattern as JIM7. That is, it labeled the primary cell wall/middle lamellae of microsporocytes and the cell walls of surrounding tissues, but failed to label post-meiotic cell plates and the newly formed microspore cell walls (Fig. 11d). In contrast, the JIM13 monoclonal antibody, which presumably recognizes the trisaccharide D-GlcA-β-1-3-D-GalA-α-1-2-Rha (Yates et al. 1996), gave a strong labeling pattern on primary cell wall/middle lamellae, callosic microsporocyte cell wall, and tapetal cell walls. However, the JIM13 antibody did not label either the Golgi stacks or Golgi-derived vesicles, or the tubular network stage of forming cell plates. Only after fusion of the wide tubular networks to the plasma membrane could JIM13 epitopes be detected over the convoluted sheets, and as these cell wall domains matured more labeling was observed. It is interesting to note that in the convoluted sheet domains the JIM13 epitopes appear to be associated initially with the membrane (see Fig. 11f, black arrowheads), whereas

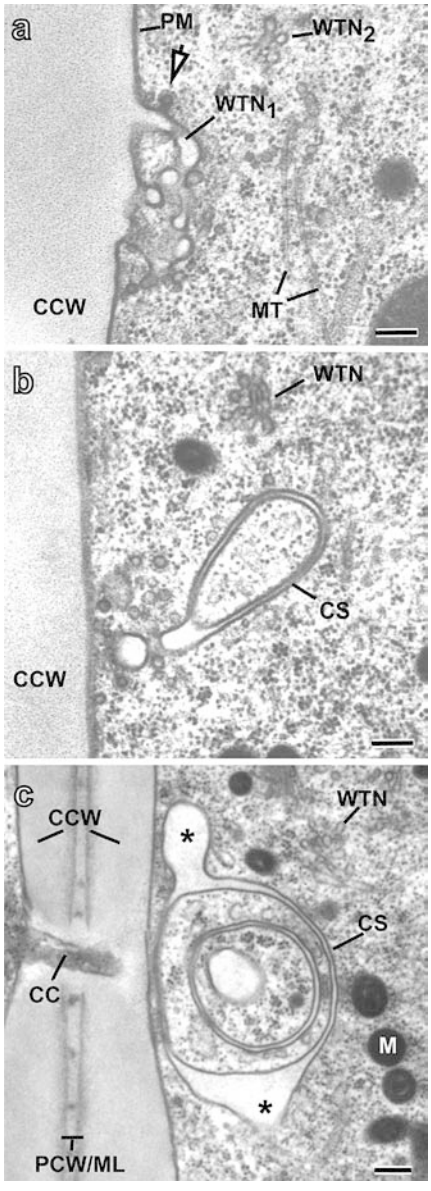

Fig. 8a–c Thin-section electron micrographs of post-meiotic cell plate intermediates. **a** A wide tubular network (WTN_1) in the process of fusing with the parental plasma membrane (*PM*). A clathrin-coated bud (*arrow*) is budding off the fusing tubes. Another wide tubular network (WTN_2) is seen in the vicinity of the already fused one. **b** Convoluted sheet domain (*CS*) already fused to the parental plasma membrane. A WTN not connected to the convoluted sheet can be seen in the upper part of this micrograph. **c** A convoluted sheet domain (*CS*) consisting of three concentric layers is fused to the parental plasma membrane, in close proximity to a cytoplasmic channel (*CC*). Note that the outer sheet exhibits swollen domains (*asterisks*). *CCW* Callosic cell wall, *M* mitochondrion, *PCW/ML* primary cell wall/middle lamellae. Bars = 200 nm

at later stages increasing amounts of the label were seen over the callosic cell wall, i.e., away from the plasma membrane (Fig. 11g, empty arrowheads).

Finally, the MAC207 monoclonal antibody, which appears to recognize an oligosaccharide that contains a terminal arabinose and glucuronic acid (Yates et al. 1996), did not label any microsporocyte cell wall or cell plates (data not shown). It only labeled cell walls of the anther wall and tapetal cells (data not shown).

Endoplasmic reticulum (ER) cisternae are closely associated with convoluted sheets

The overall low density of MTs that are involved in post-meiotic cell plate assembly allows other organelles such as mitochondria, Golgi stacks, plastids, multivesicular bodies, and even vacuoles, which are usually excluded from the division plane in somatic cells, to be in close proximity to the developing cell plate (Fig. 2; note: mitochondria are not shown for clarity).

The ER cisternae are evenly distributed across the cytoplasm at the onset of microsporocyte cellularization and do not show any specific association with early stages of cell plate assembly such as wide tubules and wide tubular networks (Fig. 2). However, ER cisternae become closely associated with convoluted sheet domains of post-meiotic cell plates (Fig. 9a,b). This association is particularly evident in the tomographic reconstruction shown in Fig. 9b, in which the ER cisternae are tightly apposed to the surfaces of the concentrically organized convoluted sheet membranes.

Discussion

In this study, we have used a combination of high-pressure freezing/freeze substitution and dual-axis electron tomography techniques to re-evaluate the cytokinetic mechanism that operates after male meiosis in *Arabidopsis*. We have found that this process involves cell plate formation and not cleavage furrows, as previously thought. However, in contrast to somatic- and endosperm syncytial-type cell plates, post-meiotic cell plates show a unique centripetal pattern of maturation. We have also visualized linkers that connect cell plate-forming vesicles with each other, demonstrated that a cell plate-forming matrix is recruited to the mini-phragmoplast sites together with the first vesicles, and shown that callose synthesis is triggered only after fusion of the most peripheral wide tubular network domains with the parental plasma membrane. A diagram illustrating the structural intermediates of post-meiotic cell plate formation is presented in Fig. 12.

Post-meiotic cell plates grow and mature centripetally but not via cleavage furrows

Arguably, the most interesting difference between cell plate formation in somatic and syncytial endosperm cells on one hand, and cell plate formation in post-meiotic cells on the other, pertains to their pattern of maturation. Whereas in somatic- and in syncytial-type cell plates maturation occurs in a centrifugal manner,

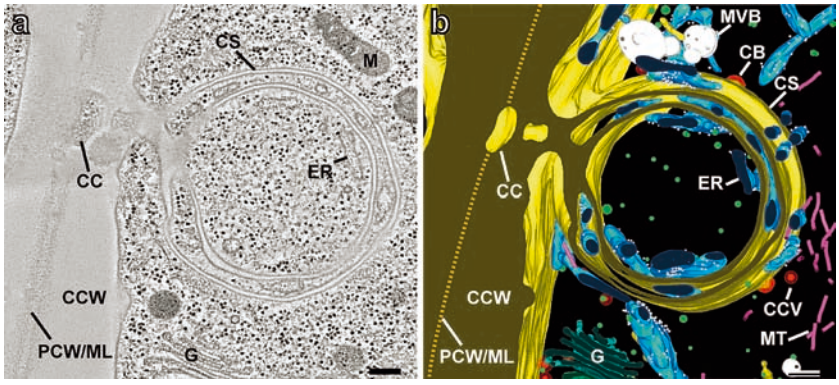

Fig. 9a, b Tomographic analysis of a convoluted sheet assembled in close proximity to a cytoplasmic channel in an *Arabidopsis* microsporocyte. **a** A 12-nm-thick tomographic slice (slicer views of four integrated 3-nm slices) through a convoluted sheet domain (*CS*) fused to the microsporocyte cell wall. This convoluted sheet consists of two concentric layers (compare to Fig. 8c). **b** Tomographic model derived from the tomogram shown in **a**. Note the close apposition of the endoplasmic reticulum (*ER*) to the CS membrane. *CB* Clathrin-coated bud, *CC* cytoplasmic channel, *CCV* clathrin-coated vesicles, *CCW* callosic cell wall, *G* Golgi, *M* mitochondrion, *MVB* multivesicular bodies, *PCW/ML* primary cell wall/middle lamellae. Bars = 100 nm

the opposite is true for post-meiotic cell plates, i.e., they display a centripetal maturation pattern. This finding makes post-meiotic cell plates unique. It is also somewhat unexpected considering that both post-meiotic microsporocytes and endosperm cells are syncytial cells that employ very similar structures in the cytokinetic process. Thus, in both systems, the sites of assembly of the new cell walls are defined by the boundaries of the nuclear-cytoplasmic domains, where MTs radiating from the surfaces of adjacent nuclei meet (Fig. 1d; Brown and Lemmon 2001a). Small clusters of these MTs then give rise to mini-phragmoplasts (Otegui and Staehelin 2000b), which bring Golgi-derived vesicles to the division plane and induce them to fuse.

The critical difference between the two syncytial systems appears to be the distribution of the initial mini-phragmoplasts between the nuclei. In the endosperm, most of the initially formed mini-phragmoplasts arise towards the central region between pairs of nuclei, and only during the later stages of cell plate assembly are the mini-phragmoplasts displaced towards the cell periphery. In contrast, the mini-phragmoplasts in the microsporocytes assemble simultaneously across the entire division plane, including the spaces adjacent to the plasma membrane (Figs. 1d, 2). Upon formation of the first wide tubular networks, those in the cell periphery soon abut against and fuse with the plasma membrane before they have linked up with the tubular networks in the interior of the cell. Because fusion of a wide tubular network with the plasma membrane triggers callose formation within the tubules and their conversion into convoluted cell plate sheets, post-meiotic cell plate maturation occurs in a centripetal direction. However, these inward-growing cell plate domains do not correspond to cleavage furrows, because their growth is mediated by fusion with preformed cell plate intermediates, the wide tubular networks, and not by the addition of individual secretory vesicles as described for cleavage furrow growth (Edamatsu 2001).

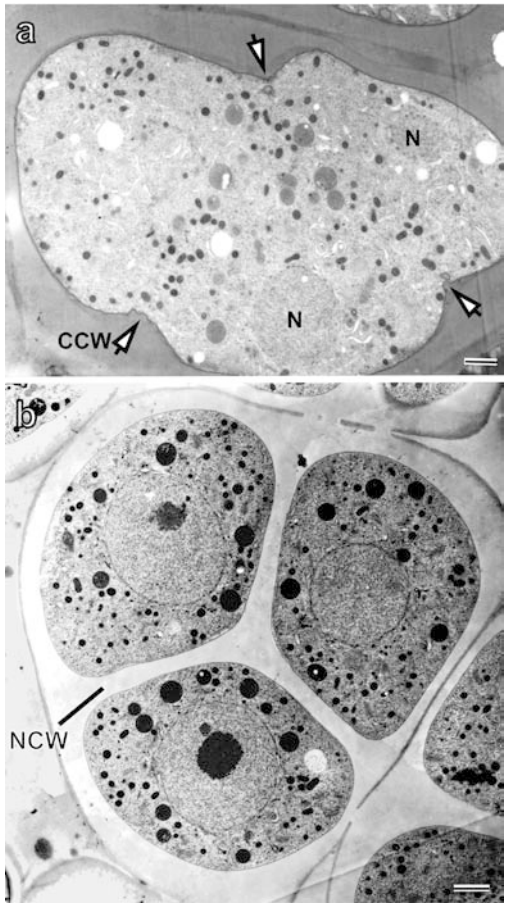

Fig. 10a, b Thin-section electron micrographs of the final steps in *Arabidopsis* microsporocyte cellularization. **a** Stub-like projections (*arrows*) extend from the parental plasma membrane/callosic cell wall (*CCW*) toward the center of the syncytium. *N* Nucleus. **b** Recently cellularized microspore tetrad. Note the thickness of the new cell walls (*NCW*) formed between microspores, and their lack of plasmodesmata and middle lamellae. Bars = 1 μm

Table 1 Labeling of cell plates and cell walls (*CWs*) with antibodies and a cellulose-specific probe during development of *Arabidopsis thaliana* pollen. At least six sections and ten micrographs were considered for immunogold analysis. When the labeling was significantly higher than the background (as determined by ANOVA and comparison of means by Tukey's test, $P < 0.05$) but the average of gold particle density was lower than three per 1 μm^2 of cell wall or lower than two gold particles per organelle, the labeling was considered "very low". Higher gold particle densities were considered as positive labeling. + Positive labeling, – no labeling, *v.l.c.* very low concentration of gold particles, *GalA* galacturonic acid, *Glc* glucose, *GlcA* glucuronic acid, *Rha* rhamnose, *t-Ara terminal arabinose*, *XG* xyloglucan

Antibody/probe	Epitopes/specificity	Cellularizing microsporocytes		Recently formed CWs in young tetrads	Microsporocyte CWs		CWs of surrounding anther tissues
		Golgi stacks and Golgi-derived vesicles	Post-meiotic cell plates		Primary CW-middle lamella	Callosic CW	
Anti-XG	β-1,4-Glc backbone of XG	v.l.c.	v.l.c.	v.l.c	v.l.c	v.l.c	+
JIM7	Methyl-esterified pectins	v.l.c	v.l.c	v.l.c	+	v.l.c	+
Anti-callose	β-1,3-Glucans	–	+	+	–	+	–
Cellulose-binding probe	Cellulose	–	–	–	–	–	+
JIM13	AGPs containing D-GlcA-β-1-3-D-GalA-α-1-2-Rha	–	– (early stages) + (late stages)	+	+	+	+
LIM2	AGP containing GlcA	–	–	–	+	–	+
MAC207	AGP containing t-Ara and D-GlcA acid	–	–	–	–	–	+

Callose synthesis is triggered by cell plate fusion with the plasma membrane

Callose synthesis occurs during development of both somatic- and syncytial-type cell plates (Samuels et al. 1995; Otegui and Staehelin 2000b). In these systems, callose synthesis is initiated after the cell plate-forming vesicles have fused into a coherent tubulo-vesicular network (somatic-type cell plates; Samuels et al. 1995) or a wide tubular network (syncytial-type cell plates; Otegui and Staehelin 2000b). In both systems, one of the main functions of callose synthesis appears to be to provide the spreading forces that drive the conversion of membrane tubules into membrane sheets as postulated by Samuels et al. (1995). Our present study on cellularizing microsporocytes supports this hypothesis, since wide tubular networks of post-meiotic cell plates that have not fused with the plasma membrane lack callose and never mature beyond the wide tubular network stage.

The enzymes that produce cell plate callose are transported in Golgi-derived vesicles to the forming cell plate in an inactive form, where a Ca^{2+} signal appears to cause their activation (Verma 2001). This tight regulation of callose synthase activity is of critical importance for cell plate maturation. In somatic- and syncytial-type cell plates, the Ca^{2+} needed for this activation is most likely released from the ER, which always encompasses these cell plates (Hepler 1982; Cutler and Ehrhardt 2002; Rancour et al. 2002). In contrast, the wide tubular networks of post-meiotic cell plates are neither surrounded by ER (Fig. 2) nor do they accumulate callose (Fig. 11a). Callose only appears in the cell plate intermediates after they have fused with the plasma membrane, suggesting that the activating Ca^{2+} comes from the cell wall.

Post-meiotic cell plates differ from syncytial-type cell plates by their lack of constricting dynamin rings and the absence of planar fenestrated sheets

The different stages of post-meiotic cell plate assembly and maturation are illustrated in Fig. 12. Most of these structural intermediates resemble those reported for syncytial-type cell plate assembly, with the exception of two striking differences. Whereas, the tomographic analysis of syncytial-type cell plates in the endosperm has shown the presence of ADL1A (*Arabidopsis* dynamin-like protein 1A) rings constricting the membranes of the wide tubular network domains (Otegui et al. 2001), no such rings were detected in wide tubules of post-meiotic cell plates (Fig. 7). This lack of constricting dynamin rings may reflect on the fact that each nuclear cytoplasmic domain in the microsporocyte has to produce only three relatively small half cell walls (approx. 7 μm×7 μm), versus six large half cell walls in the syncytial endosperm (20 μm×20 μm, Otegui et al. 2001). Thus, cell plate assembly most likely occurs much faster,

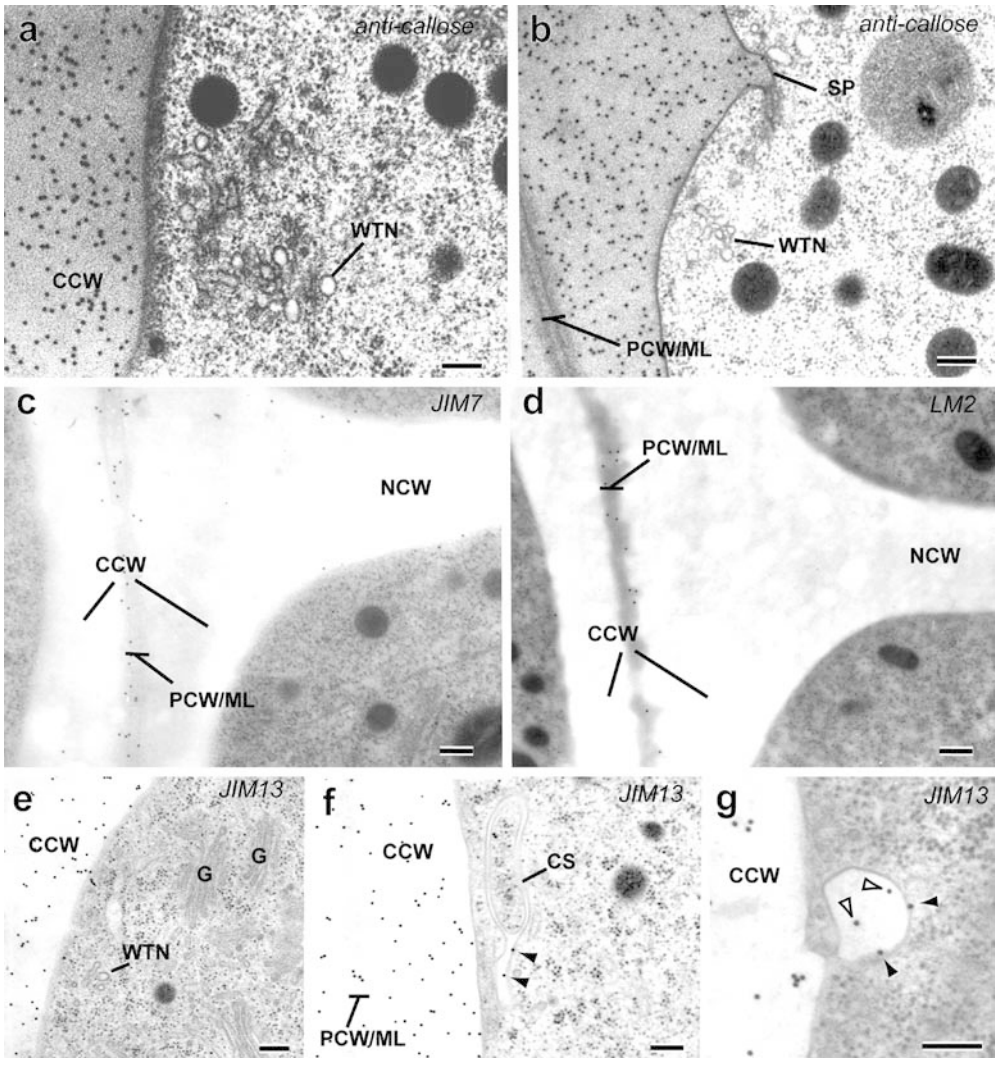

Fig. 11a–g Labeling of *Arabidopsis* microsporocyte cell plates and cell walls with specific antibodies. **a** Section of a wide tubular network (*WTN*) and callosic cell wall (*CCW*) labeled with anti-callose antibody. Note the lack of label on the wide tubular network domains. **b** Section of a cellularizing microsporocyte labeled with anti-callose antibody. The stub-like projection (*SP*) growing toward the interior of the syncytium is heavily labeled whereas the individual wide tubular networks (*WTN*) assembled across the division plane are not. **c** Section of a recently formed tetrad labeled with JIM7. **d** Section of a recently formed tetrad labeled with LM2. **e** Section through the division plane at the onset of post-meiotic cell plate assembly labeled with JIM13. Golgi stacks (*G*) and wide tubules are not labeled. **f** Section of a convoluted sheet (*CS*) and microsporocyte cell wall labeled with JIM13. Note the label on the convoluted sheet membrane (*black arrowheads*). **g** Section of a stub-like projection labeled with JIM13. Note that label is present both over the membrane (*black arrowheads*) and over the stub-like projection/cell wall (*empty arrowheads*). *CCW* Callosic cell wall, *NCW* newly formed cell wall, *PCW*/*ML* primary cell wall/middle lamellae. Bars = 100 nm

and dynamin rings are not critical for maintaining the tubular architecture of the wide tubular networks over prolonged periods of time. However, we cannot rule out the possibility that there are dynamin-like proteins associates with post-meiotic type cell plates but we could not find any evidence for such rings in our tomograms.

The other structural difference between syncytial- and post-meiotic-type cell plates pertains to the absence of a distinct planar fenestrated sheet stage in the latter. Instead, as the convoluted sheets accumulate more callose and AGPs, the projections that originate at the cell periphery convert directly into callose-rich cell walls.

Vesicle-bridging structures appear to be transported together with the vesicles and the cell plate assembly matrix to the forming cell plate sites

Our tomographic models contain numerous membranous structures that appear to be derived from the fusion of two or three vesicles, or of a vesicle and a short tubule (Fig. 4g–i). In the same areas, we have also observed rod-like structures connecting two or more vesicles and membranous tubules together (Figs. 3a,b, 4a–f). Recent studies have shown that the process of vesicle fusion involves several protein complexes, each of which serves a specific function. Best known are the SNARE

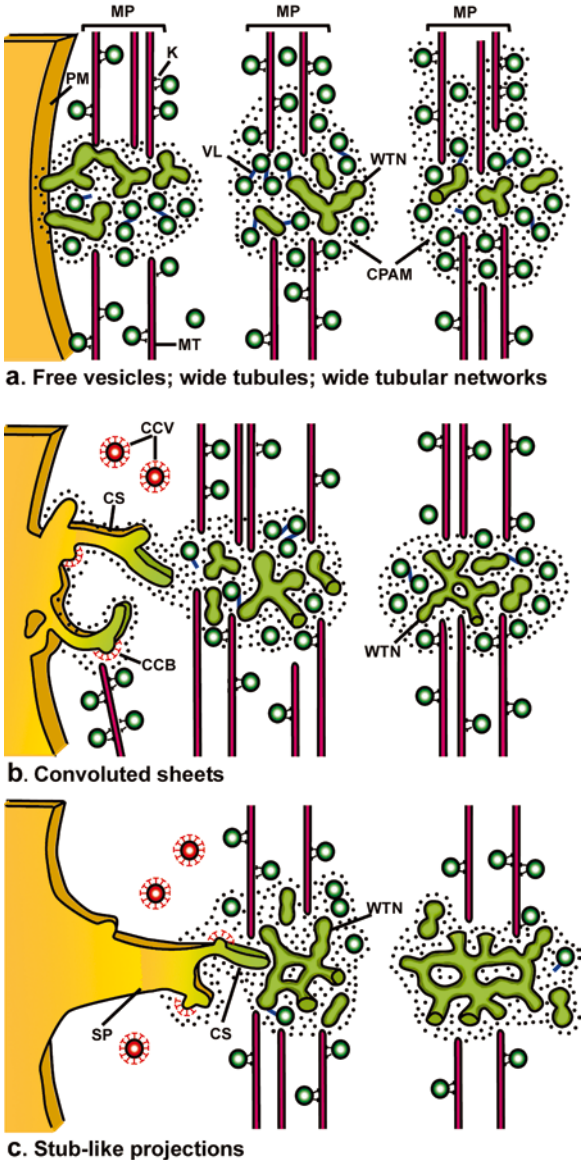

Fig. 12 Main developmental stages of post-meiotic cell plate assembly. The model depicts the main stages in post-meiotic cell plate assembly during microsporocyte cellularization in *Arabidopsis*. *CCB* Clathrin-coated bud, *CCV* clathrin-coated vesicles, *CS* convoluted sheet, *K* kinesin, *CPAM* cell plate assembly matrix, *MP* mini-phragmoplasts, *PM* plasma membrane, *SP* stub-like projection, *VL* vesicle-linkers, *WTN* wide tubular networks

proteins and a variety of tethering factors, which contribute both to the specificity of membrane docking and to the membrane fusion process (Guo et al. 2000). The exocyst, one of the best-characterized tethering factors, localizes to sites of polarized exocytosis (Whyte and Munro 2002). In mammalian cells, it consists of eight subunits: Sec3p, Sec5p, Sec6p, Sec8p, Sec10p, Sec15p, Exo70p, and Exo84p (Lipschutz and Mostov 2002; Whyte and Munro 2002). Cytokinesis in all eukaryotic cells appears to involve vesicle fusion at specific sites, and thus it could be considered as a case of polarized exocytosis. Indeed, the exocyst complex has been shown to be required for completion of cytokinesis in a variety of eukaryotic cells. For example, in mutant *sec8-1* cells of *Schizosaccharomyces pombe*, clusters of vesicles accumulate in the vicinity of the forming septa, suggesting that targeting of the vesicles to the division plane is normal but subsequent vesicle docking/fusion is impaired (Wang et al. 2002).

Recently, several exocyst subunits have been identified in plants (Elias et al. 2003), but their functional roles during exocytosis and cytokinesis have yet to be characterized. We speculate that the vesicle-linkers seen in our tomograms could be exocyst-type tethering factors. Support for this hypothesis has come from the finding that the tethering rods in post-meiotic cell plates have a bridging length of approx. 24 nm, which is similar to the length of isolated, glutaraldehyde-fixed rat exocyst complexes visualized by quick-freeze, deep-etch electron microscopy (Hsu et al. 1999).

In our previous tomographic analysis of syncytial-type cell plates we did not observe any vesicle-linkers (Otegui et al. 2001), most likely due to the very low density of vesicles found at the cell plate assembly sites during endosperm cellularization. However, it is likely that vesicle-linkers are present in all types of cell plate.

Interestingly, the vesicle-linkers observed in our tomograms were always found inside the limits of the cell plate assembly matrix. We have postulated previously (Otegui et al. 2001) that this matrix, which surrounds the growing domains of somatic (Samuels et al. 1995) and syncytial (Otegui et al. 2001) types of cell plate, could create the local conditions conductive for both membrane fusion and recycling, and therefore, cell plate assembly. In the present study, we have also demonstrated that the matrix material is transported together with the first vesicles to the division plane, which further supports the idea of a functional role of the matrix during cell plate assembly.

The unusual composition of post-meiotic cell plates and newly formed cell walls reflects their transient nature and their unique functional attributes

In contrast to somatic- and syncytial-type cell plates, post-meiotic cell plates do not contain detectable amounts of cellulose, xyloglucans, or methyl-esterified pectins. In addition, callose and AGPs recognized by the JIM13 antibody become detectable only after the individual cell plates assembly sites fuse with the plasma membrane. Whereas the unusual pattern of callose synthesis could be due to a late activation of the callose synthase complexes (see above), the absence of JIM13 labeling on Golgi stacks, vesicles and wide tubular networks is harder to explain. The JIM13 antibody used in this study recognizes a specific epitope in the glycosidic portion of AGPs (Knox et al. 1991). The JIM13 labeling pattern obtained from post-meiotic cell plates suggests that the JIM13 epitope only becomes available for immunodetection after the cell plate fuses with the plasma

membrane. This may be due to a late modification in the glycosidic part of the AGP during cell plate maturation.

The classical group of AGPs are known to be attached to the plasma membrane by glycosylphosphatidylinositol anchors (Schultz et al. 2002). They can also be released into the cell wall by specific lipases (Showalter 2001). The AGP recognized by the JIM13 antibody in our study appears to follow this pathway. Thus, when the JIM13 epitope-containing AGPs are first detected in convoluted sheets, the labeling appears over the plasma membrane and only later over the cell plate/cell wall. This observation suggests that the JIM13 antibody recognizes a lipid-linked AGP, whose anchor is cleaved after it reaches the plasma membrane.

Once cytokinesis has been completed, thick cell walls separate the four microspores in every tetrad. These new cell walls exhibit several unique features, including a complete lack of plasmodesmata and a very high content of callose and AGPs. In addition, no middle lamella can be detected between adjacent microspores. The uniqueness of these cell walls is likely related to their transient nature and their specific functional attributes. Immediately after the tetrad is established, every microspore begins to form the future pollen grain wall, starting with the outer layer, the exine. The building of the exine starts with the assembly of the primexine matrix between the plasma membrane and the callosic cell wall. Shortly thereafter, the callosic cell wall that surrounds the microspores is completely degraded, the microspores released, and the primexine accumulates the sporopollenin precursors secreted by the tapetum. Thus, the cell walls formed after meiosis between microspores have to be both deformable, to allow the development of the primexine, and easy to degrade. Both callose and AGPs are known for their gel-forming properties and their rapid rates of turnover (Showalter 2001; Verma and Hong 2001), and thus, the unique composition of the initially formed microspore cell walls reflects the requirements for a transient structural intermediate in pollen wall assembly.

Acknowledgements This work was supported by National Institute of Health Grant 59787 to L.A.S. and by grants from the Antorchas Foundation and IM40 Agencia de Promocion Cientifica y Tecnologica to M.S.O. M.S.O. is a researcher at Consejo Nacional de Investigaciones Científicas y Técnicas.

References

Brown RC, Lemmon BE (1991a) Pollen development in orchids. I. Cytoskeletal control of division plane in irregular pattern of meiotic cytokinesis. Protoplasma 163:9–18

Brown RC, Lemmon BE (1991b) The cytokinetic apparatus in meiosis: control of the division plane in the absence of a preprophase band of microtubules. In: Lloyd CW (ed) The cytoskeletal basis of plant growth and form. Academic Press, London, pp 259–273

Brown RC, Lemmon B (1996) Nuclear cytoplasmic domains, microtubules and organelles of the slipper orchid *Cypripedium californicum* A Gray dividing by simultaneous cytokinesis. Sex Plant Reprod 9:145–152

Brown RC, Lemmon BE (2000) The cytoskeleton and polarization during pollen development in *Carex blanda* (Cyperaceae). Am J Bot 87:1–11

Brown RC, Lemmon BE (2001a) Phragmoplasts in the absence of nuclear division. J Plant Growth Regul 20:151–161

Brown RC, Lemmon BE (2001b) The cytoskeleton and spatial control of cytokinesis in the plant life cycle. Protoplasma 215:35–49

Cutler SR, Ehrhardt DW (2002) Polarized cytokinesis in vacuolated cells of *Arabidopsis*. Proc Natl Acad Sci USA 99:2812–2817

Edamatsu M (2001) The molecular mechanism of targeted vesicles transport in cytokinesis. Cell Struct Funct 26:567–570

Elias M, Drdova E, Ziak D, Bavlnka B, Hala M, Cvrckova F, Soukupova H, Zarsky V (2003) The exocyst complex in plants. Cell Biol Int 27:199–201

Gilbert PFC (1972) The reconstruction of a three-dimensional structure from projections and its application to electron microscopy. II. Direct methods. Proc R Soc Lond B 182:89–102

Guo W, Sacher M, Barrowman J, Ferro-Novick S, Novick P (2000) Protein complexes in transport vesicle targeting. Trends Cell Biol 10:251–255

Hepler PK (1982) Endoplasmic-reticulum in the formation of the cell plate and plasmodesmata. Protoplasma 111:121–133

Hirokawa N, Pfister KK, Yorifuji H, Wagner M, Brady S, Bloom G (1989) Submolecular domains of bovine brain kinesin identified by electron microscopy and monoclonal antibody decoration. Cell 56:867–878

Hsu S-C, Hazuka CD, Foletti DL, Scheller RH (1999) Targeting vesicles to specific sites on the plasma membrane: the role of the sec6/8 complex. Trends Cell Biol 9:150–153

Hülskamp M, Parekh NS, Grini P, Schneitz K, Zimmermann I, Lolle S, Pruit R (1997) The STUD gene is required for male-specific cytokinesis after telophase II of meiosis in *Arabidopsis thaliana*. Dev Biol 187:114–124

Knox JP, Linstead PJ, King J, Cooper C, Roberts K (1990) Pectin esterification is spatially regulated both within cell walls and between developing tissues of root apices. Planta 181:512–521

Knox JP, Linstead PJ, Peart J, Cooper C, Roberts K (1991) Developmentally regulated epitopes of cell surface arabinogalactan proteins and their relation to root tissue pattern formation. Plant J 1:317–326

Kremer JR, Mastronarde DN, McIntosh JR (1996) Computer visualization of three-dimensional image data using IMOD. J Struct Biol 116:71–76

Krishnamurthy KV (1999) Methods in cell wall cytochemistry. CRC Press, Boca Raton

Ladinsky MS, Mastronarde DN, McIntosh JR, Howell KE, Staehelin LA (1999) Golgi structure in three dimensions: functional insights from the normal rat kidney cell. J Cell Biol 144:1135–1149

Lauber MH, Waizenegger I, Steinmann T, Schwarz H, Mayer U, Hwang I, Lukowitz W, Jürgens G (1997) The *Arabidopsis* KNOLLE protein is a cytokinesis-specific syntaxin. J Cell Biol 139:1485–1493

Lipschutz JH, Mostov KE (2002) Exocytosis: the many masters of the exocyst. Curr Biol 12:212–214

Mastronarde DN (1997) Dual-axis tomography: an approach with alignment methods that preserve resolution. J Struct Biol 120:343–352

Mineyuki Y (1999) The preprophase band of microtubules: its function as a cytokinetic apparatus in higher plants. Int Rev Cytol 187:1–49

Moore PJ, Darvill AG, Albersheim P, Staehelin LA (1986) Immunogold localization of xyloglucans and rhamnogalacturonan I in the cell walls of suspension-cultured sycamore cells. Plant Physiol 82:787–794

Otegui MS, Staehelin LA (2000a) Cytokinesis in flowering plants: more than one way to divide a cell. Curr Opin Plant Biol 3:493–502

Otegui MS, Staehelin LA (2000b) Syncytial-type cell plates: a novel kind of cell plate involved in endosperm cellularization of *Arabidopsis*. Plant Cell 12:933–947

Otegui MS, Mastronarde DN, B-HK, Bednarek SY, Staehelin LA (2001) Three-dimensional analysis of syncytial-type cell plates during endosperm cellularization visualized by high resolution electron tomography. Plant Cell 13:2033–2051

Owen HA, Makaroff CA (1995) Ultrastructure of microsporogenesis and microgametogenesis in *Arabidopsis thaliana* (L.) Heynh. ecotype Wassilewskija (Brassicaceae). Protoplasma 185:7–21

Pennel RI, Roberts K (1990) Sexual development in the pea is presaged by altered expression of arabinogalactan protein. Nature 344:547–549

Rancour DM, Dickey CE, Park S, Bednarek SY (2002) Characterization of AtCDC48. Evidence of multiple fusion mechanisms at the plane of cell division in plants. Plant Physiol 130:1241–1253

Samuels LA, Giddings TH, Staehelin LA (1995) Cytokinesis in tobacco BY-2 and root tip cells: a new model of cell plate formation in higher plants. J Cell Biol 130:1345–1357

Schultz CJ, Johnson KL, Currie G, Bacic A (2002) The classical arabinogalactan protein gene family of *Arabidopsis*. Plant Cell 12:1751–1767

Showalter AM (2001) Arabinogalactan-proteins: structure, expression and function. Cell Mol Life Sci 58:1399–1417

Smallwood M, Yates EA, Wilats WGT, Martin H, Knox JP (1996) Immunochemical comparison of membrane associated and secreted arabinogalactan-proteins in rice and carrot. Planta 198:452–459

Spielman M, Preuss D, Li FL, Browne WE, Scott, RJ (1997) *TETRASPORE* is required for male cytokinesis in *Arabidopsis thaliana*. Development 124:2645–2657

Staehelin LA, Hepler PK (1996) Cytokinesis in higher plants. Cell 84:821–824

Verma DPS (2001) Cytokinesis and building of the cell plate in plants. Annu Rev Plant Physiol Plant Mol Biol 52:751–784

Verma DPS, Hong Z (2001) Plant callose synthase complexes. Plant Mol Biol 47:693–701

Wang H, Tang X, Liu J, Trautmann S, Balasundaram D, McCollum D, Balasubramanian MK (2002) The multiprotein exocyst complex is essential for cell separation in *Schizosaccharomyces pombe*. Mol Biol Cell 13:515–529

Whyte JRC, Munro S (2002) Vesicle tethering complexes in membrane traffic. J Cell Sci 115:2627–2637

Yates EA, Valdor JF, Haslam SM, Morris HR, Dell A, Mackie W, Knox JP (1996) Characterization of carbohydrate structural features recognized by anti-arabinogalactan-protein monoclonal antibodies. Glycobiology 6:131–139